Inorg. Chem. **2009**, *48*, 3523−3528

Direct Observation of Molecular Structural Change *during* Intersystem Crossing by Real-Time Spectroscopy with a Few Optical Cycle Laser

Izumi Iwakura,[†,‡] Takayoshi Kobayashi,[*,‡,§,||,⊥] and Atsushi Yabushita[||]

JSPS Research Fellow, 8 Ichibancho, Chiyoda-ku, Tokyo 102-8472, Japan, University of Electro-Communications, 1-5-1 Chofugaoka, Chofu, Tokyo 182-8585, Japan, ICORP, JST, 4-1-8 Honcho, Kawaguchi, Saitama, 332-0012, Japan, Department of Electrophysics, National Chiao-Tung University, Hsinchu 30010, Taiwan, and Institute of Laser Engineering, Osaka University, 2-6 Yamada-oka, Suita, Osaka 565-0971, Japan

Received April 24, 2008

Ultrafast spectroscopy by a sub-5 fs pulse laser was applied to the simultaneous study of electronic relaxation and vibrational dynamics in Ru^{II}(TPP)(CO). The electronic lifetimes of $^1Q_{x(1,0)}(\pi,\pi^*)$ and $^1Q_{x(0,0)}(\pi,\pi^*)$ were determined to be 230 ± 70 fs and 1150 ± 260 fs, respectively. The spectrogram shows the time dependent changes in the vibrational spectrum associated with the spin state change from the Franck−Condon state in the excited singlet state to the triplet state via the curve crossing point between the singlet and triplet potential surfaces. The time constant of the intersystem crossing process was determined to be about 1.0 ps from observed electronic relaxation and vibrational dynamics reflecting the transition from the singlet to triplet electronic excited state.

Introduction

Metallo-porphyrin complexes have been extensively studied as model complexes for many important biological systems. The report of the oxidation reaction of Ru^{II}(TPP)(CO) [TPP = tetraphenylporphyrin] in 1973[1] triggered numerous studies of Ru^{II}(TPP)(CO) as a model complex of Fe^{II}(por) [por = porphyrin], a central skeleton of hemoglobin which functions as an oxygen transport in human bodies. However, detailed studies have not yet been conducted on the excited-state dynamics of Ru^{II}(TPP)(CO). It is known that the lowest excited triplet state in Ru^{II}(CO) porphyrin is $^3(\pi,\pi^*)$,[2] and the phosphorescence lifetime in Ru^{II}(TPP)(CO)(py) [py = pyridine] was measured to be 35 μs at room temperature.[3] The fluorescence lifetime has not been yet resolved, but it was reported to be shorter than 30 ps in 1999[3] and 1 ps in 2005.[4] The electronic excited state relaxes via vibronic coupling; therefore, information of pure electronic dynamics is not enough to elucidate the relaxation process of the electronic excited states.[5] The real-time vibrational spectroscopy provides the modulated probability of electronic transition by molecular vibration. By this method, we can obtain both the information on the radiation-less electronic relaxation and on the instantaneous vibrational frequency during the relaxation while at the same time using a single experimental system, satisfying completely the same experimental conditions.

Experimental Section

Broadband Visible Pulse Generation by NOPA. Using a noncollinear optical parametric amplifier (NOPA) shown in Figure 1, we obtained an ultra-broadband visible pulse, which can be compressed to sub-5 fs for the ultrafast pump−probe measurement.

As a laser source, a Ti:sapphire regenerative amplifier (Spectra-Physics, model Spitfire, 150 μJ, 100 fs, 5 kHz at 805 nm) was

* To whom correspondence should be addressed. E-mail: kobayashi@ils.uec.ac.jp.
† JSPS Research Fellow.
‡ University of Electro-Communications.
§ ICORP, JST.
|| National Chiao-Tung University.
⊥ Osaka University.

(1) Brown, G. M.; Hopf, F. R.; Ferguson, J. A.; Meyer, T. J.; Whitten, D. G. J. *J. Am. Chem. Soc.* **1973**, *95*, 5939–5942.
(2) (a) Rillema, D. P.; Nagle, J. K.; Barringer, L. F.; Mayer, T. J. *J. Am. Chem. Soc.* **1981**, *103*, 56–62. (b) Levine, L. M. A.; Holten, D. *J. Phys. Chem.* **1988**, *92*, 714–720. (c) Antipas, A.; Buchler, J. W.; Gouterman, M.; Smith, P. D. *J. Am. Chem. Soc.* **1978**, *100*, 3015–3027.
(3) Prodi, A.; Indelli, M. T.; Kleverlaan, C. J.; Scandola, F.; Alessio, E.; Gianferrara, T.; Marzilli, L. G. *Chem.—Eur. J.* **1999**, *5*, 2668–2679.
(4) Prfodi, A.; Chiorboli, C.; Scandola, F.; Iengo, E.; Alessio, E.; Dorbrawa, R.; Würthner, F. *J. Am. Chem. Soc.* **2005**, *127*, 1454–1462.
(5) Iwakura, I.; Yabushita, A.; Kobayashi, T. *Eur. J. Inorg. Chem.* **2008**, 4856–4860.

10.1021/ic801477a CCC: $40.75
Published on Web 03/16/2009

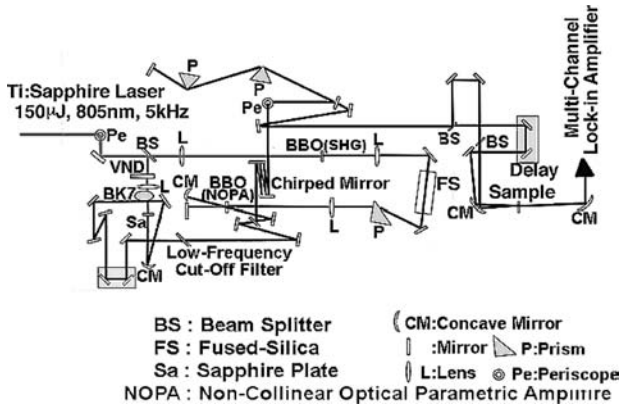

Figure 1. NOPA for sub-5 fs pump−probe measurement system.

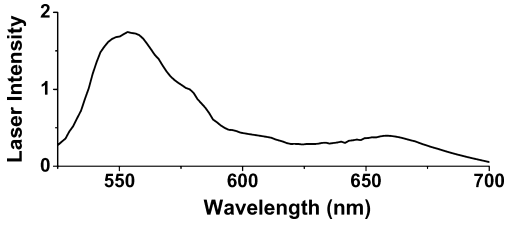

Figure 2. Laser spectrum of the sub-5 fs pulses used for pump pulse and probe pulse extending from 525 to 725 nm.

used to generate pump and seed pulses of NOPA. A single-filament white light continuum was generated in a 1 mm-thick sapphire plate to be used as the seed pulse. The seed pulse was non-collinearly amplified in a NOPA crystal (type I-BBO, $\theta = 31.5°$) pumped by a second harmonic (SH, 100 μJ) of the laser source. The SH used for the pump pulse of NOPA was generated by a 0.4 mm-thick BBO crystal to obtain broadband SH pulse.

After amplification in NOPA, a main compressor compensates the residual chirp. The total pulse compressor is composed of the ultra-broadband chirped mirror (UBCM, Hamamatsu Photonics) pair, a 45° fused-silica prism pair, and 0.5 mm-thick Cr-coated broadband beam-splitters. The UBCM pair with three round trips and prism pair are for the main compression. The amplified signal pulse after the double-pass NOPA with a spectrum extending from 525 to 725 nm was compressed with the main compressor resulting in a pulse duration of sub-5 fs which is nearly Fourier transform limited.

Pump−Probe Measurement. We used a sub-5 fs pulse[6] to observe the real-time vibrational dynamics associated with relaxation in the electronic states of Ru^{II}(TPP)(CO) in $CHCl_3$, a non-coordinating solvent.[7] The spectrum of the sub-5 fs pulses covered from 525 to 725 nm with a nearly constant phase (Figure 2). The polarizations of the pump and the probe beams were parallel to each other. The intensities of the pump and probe pulses were 2880 ± 300 and 480 ± 50 GW cm^{-2}, respectively. The focus areas of the pump and probe pulses were 100 μm^2 and 75 μm^2, respectively.

All measurements were performed at 295 ± 1 K using a sample solution in a 1 mm cell. Time-resolved difference transmittance ΔT in the spectral range extending from 525 to 700 nm was measured simultaneously using a multichannel lock-in amplifier coupled to a polychromator (300 grooves/mm, 500 nm blazed)

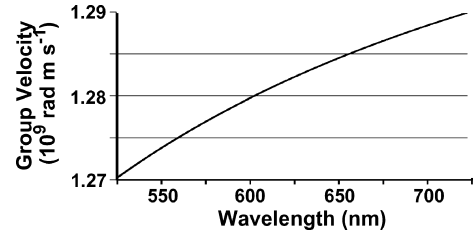

Figure 3. Group velocity dispersion of chloroform.

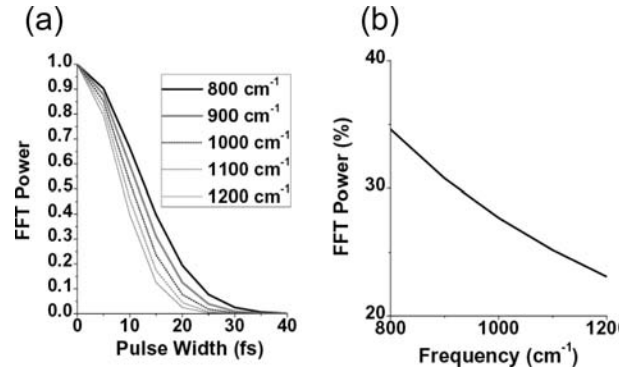

Figure 4. (a) Simulation result to show the effect of reduction of the normalized FFT power of real-time traces with vibration frequencies from 800 to 1200 cm^{-1} measured with different pulse widths from 0 to 40 fs. (b) Simulation result of the loss in the observed FFT power of the vibration modes from 800 to 1200 cm^{-1} measured for chloroform in a 1 mm cell.

coupled to avalanche photodiodes through a 112-channel fiber bundle. The spectral resolution of the system was about 1.57 nm. The transmitted probe spectrum after the sample without the injection of the pump was recorded by averaging 50,000 laser shots. The transmission difference of the probe was accumulated every 3,000 laser shots under the excitation conditions by the pump pulse. The pump−probe experiment was performed with a 1 fs step from −100 to 4,800 fs.

Group Velocity Dispersion (GVD). The refractive index of chloroform is $n = 1.431364 + 5632.41/\lambda^2 - 2.0805 \times 10^8/\lambda^4 + 1.2613 \times 10^{13}/\lambda^{6.8}$ Therefore, the GVD of chloroform is calculated as Figure 3. The pulse width after transmission through a 1 mm cell was calculated to be about 40 fs.

Since the electronic relaxation time to be discussed in this paper was found to be longer than 200 fs, the effect of GVD on the electronic relaxation dynamics is negligible. On the other hand, the effect in vibrational dynamics can be substantial because the stretched pulse width attenuates the amplitude of the molecular vibration observed in the signal as shown in Figure 4a. Vibration modes with frequencies between 800 and 1200 cm^{-1} discussed in this article are reduced in their amplitudes because of their short vibrational period, which cannot be properly resolved by the stretched pulse having similar to or longer duration than the vibrational periods. However, the value of vibration frequency is not affected. Hence, the frequency and its shift can still be correctly discussed even with observation by the stretched pulse. As is seen in Figure 4a, the effect of pulse width is almost the same in the vibration frequencies from 800 to 1200 cm^{-1}. The amplitude of high frequency modes were corrected using the calculated results shown in Figure 4b.

Robustness of the Sample against Laser Irradiation. The (d,π^*) excitation induces the π back-donation of Ru(dπ)→CO(π^*)

(6) (a) Kobayashi, T.; Shirakawa, A. *Appl. Phys. B: Laser Opt.* **2000**, *70*, S239−S-246. (b) Baltuska, A.; Fuji, T.; Kobayashi, T. *Opt. Lett.* **2002**, *27*, 306–308.

(7) (a) Kadish, K. M.; Chang, D. *Inorg. Chem.* **1982**, *21*, 3614–3618. (b) Kadish, K. M.; Leggett, D. J.; Chang, D. *Inorg. Chem.* **1982**, *21*, 3618–3622.

(8) Samoc, A. *J. Appl. Phys.* **2003**, *94*, 6167–6174.

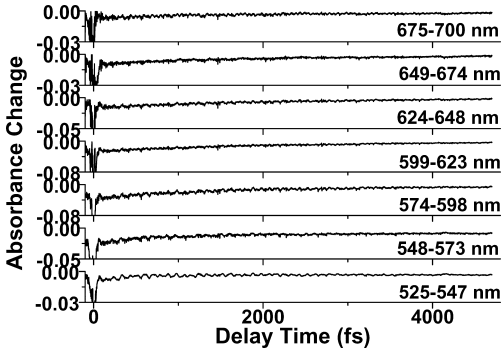

Figure 5. Real-time traces of induced absorbance changes of Ru^{II}(TPP)(CO) averaged over 16 probe channels in the delay time range between −100 and 4800 fs.

and photodissociates CO with a quantum yield of 1.9×10^{-4}.[2b,9] To investigate the effect of photodissociation in the procedure of pump−probe experiment, we estimated the rate of photodissociation of Ru(por)CO. After being excited by a single laser pulse, 8×10^5 of Ru(por)CO molecules are to be photodissociated. The experimental time required for the photodissociation of 10% of Ru(por)CO was then calculated to be about 24 s. While the Stokes equation f [kg s^1] $= 6\pi a\eta$, where the radius of Ru porphyrin a and the viscosity of chloroform η are 1.8×10^{-9} m and 0.57×10^{-3} kg m^{-1} s^{-1}, respectively, and diffusion coefficient D [m^2 s^1] $= kT/f$ can give the calculated result that the diffusion length of the molecule is about 50 μm in 24 s, which induces 125-times dilution of the photodissociated molecule. Therefore, the above calculation shows that the effect of the photodissociation is negligible.

In addition, we found that the absorption spectrum did not change before and after the experiment.

Spectroscopy. Ultraviolet/Visible (UV/vis) spectra were recorded on a Shimadzu model UV-3101PC spectrometer. Emission spectra were recorded on a HITACHI model F-4500 fluorescence spectrophotometer.

Results

Real-time traces from −100 to 4800 fs of the absorbance change (ΔA) and probe wavelength dependency of ΔA (525−700 nm) obtained in the pump−probe measurement are shown in Figures 5 and 6, respectively. Figure 6 shows that the difference absorption spectrum ($\Delta A(\omega)$). The difference absorbance, ΔA, was negative over the entire probe wavelength range in the full delay-time range. The time-resolved spectrum at delay time earlier than 1 ps has a peak wavelength and width similar to the stimulated emission spectrum ($\lambda_{max} = 595$ nm) of Ru^{II}(TPP)(CO) calculated from the fluorescence spectrum (Supporting Information, Figure S1).[10] Since the phosphorescence spectrum of Ru^{II}(TPP)-(CO)(Py) is known to be peaked at $\lambda_{max} = 726$ nm,[3] the observed emission peak at $\lambda_{max} = 595$ nm was assigned not

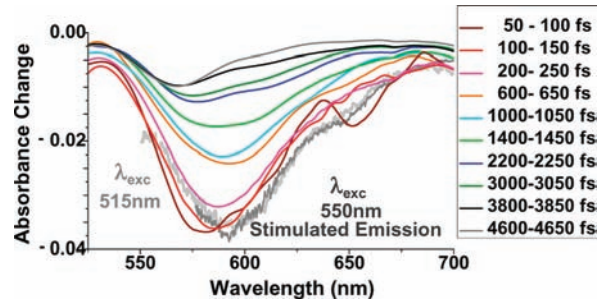

Figure 6. Difference absorption spectra of Ru^{II}(tpp)(CO) and stimulated emission spectra calculated from fluorescence spectrum.[10] The 10 ΔA spectra at different time regions were obtained by averaging for 50 fs in each time region of 50−100 fs (wine), 100−150 fs (red), 200−250 fs (pink), 600−650 fs (orange), 1000−1050 fs (cyan), 1400−1450 fs (green), 2200−2250 fs (blue), 3000−3050 fs (olive), 3800−3850 fs (black), and 4600−4650 fs (gray). Thick curves show stimulated emission spectra, whose excitation wavelengths are 515nm (dark gray) and 550nm (light gray).

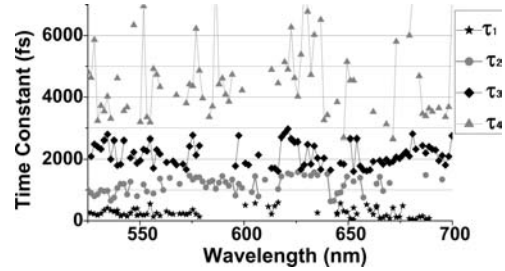

Figure 7. Probe wavelength dependence of electronic lifetimes of four excited states obtained by singular-value decomposition analysis.

to phosphorescence but to fluorescence.[11] The negative peak at 580 nm appears at a shorter delay time than 100 fs and is red-shifted to 591 nm after 100 fs. This red shift occurs at a rate of 0.67 ± 0.15 eV ps^{-1} and is considered to be due to a dynamic Stokes-shift. This corresponds to the step down time from higher vibrational levels to the lower level of the mode coupled to the electronic state. The coupled mode frequency can be calculated from the energy difference between $Q_x(1,0)$ (18939 cm^{-1}) and $Q_x(0,0)$ (17897 cm^{-1}) as 1042 cm^{-1}. Therefore, from the red-shift rate of 0.67 ± 0.15 eV ps^{-1}, the step-down time on the vibrational ladder is determined to be 1042 cm^{-1}/0.67 ± 0.15 eV ps^{-1} = 190 ± 40 fs. The ΔA signal is mainly due to the stimulated emission from $^1Q_{x(0,0)}(\pi,\pi^*)$, whose lifetime was determined by the analysis described below.

Discussion

Singular-valued decomposition (SVD) analysis of the time-resolved traces provides four decay time constants (τ_1, τ_2, τ_3, and τ_4) as shown in Figure 7. Using the average of lifetimes obtained at 112 probe wavelength channels, τ_1, τ_2, τ_3, and τ_4 were determined to be 230 ± 70 fs, 1150 ± 260 fs, 2150 ± 360 fs, and 4.6 ps, respectively. The decay time constants were obtained by fitting the time-resolved ΔA traces recorded up to the delay time of 4.8 ps. Considering limited accuracy of the fitted time constant shorter enough

(9) Sorgues, S.; Poisson, L.; Raffael, K.; Krim, L.; Soep, B.; Shafizadeh, N. *J. Chem. Phys.* **2006**, *124*, 114302.

(10) The stimulated emission spectrum was calculated from the spontaneous emission spectrum of the sample excited at $\lambda_{exc} = 515$ nm ($Q_x(1,0)$ band) and at $\lambda_{exc} = 550$ nm ($Q_x(0,0)$ band), which were recorded on a HITACHI model F-4500 fluorescence spectrophotometer, using the relation between the Einstein coefficients A_{nm} (spontaneous emission) and B_{nm}(stimulated emission) given by $A_{nm} = (2hc/\lambda^3)B_{nm}$.

(11) The fluorescence spectra ($\lambda_{max} = 560$ nm) of Ru^{II}(TPP)(CO)(dansylimidazole) (a) Lim, M. H.; Lippard, S. J. *Inorg. Chem.* **2004**, *43*, 6366–6370; That ($\lambda_{max} = 556$ nm) of Ru^{II}(OEP)(CO)(py). (b) Hopf, F. R.; O'Brien, T. P.; Scheidt, W. R.; Whitten, D. G. *J. Am. Chem. Soc.* **1975**, *97*, 277–281.

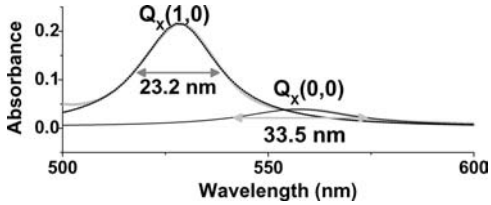

Figure 8. Visible absorption spectra of $Q_x(1,0)$ and $Q_x(0,0)$ of Ru^{II}(TPP)(CO) (gray line). They were obtained from the absorption spectrum of the sample fitted by two Lorentzian functions ($Q_x(1,0)$: black dots, $Q_x(0,0)$: black line).

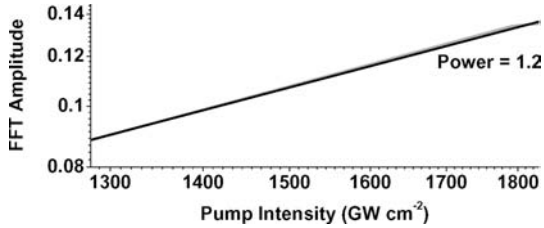

Figure 9. Pump intensity dependence of vibrational amplitude of the porphyrin ring stretching mode (1040 cm^{-1}).

than 4.8 ps, the signal component with the decay time of 4.6 ps was included in the constant component in the analysis. The UV/vis absorption spectrum of Ru^{II}(TPP)(CO) has a $Q_x(1,0)$ band peak at $\lambda_{max} = 528$ nm (18939 cm^{-1}) and a $Q_x(0,0)$ band peak at $\lambda_{max} = 560$ nm (17897 cm^{-1}) as shown in Figure 8. The laser spectrum extending from 525 to 725 nm covers both of the absorption bands; therefore, Ru^{II}(TPP)(CO) was coherently excited into both of the $^1Q_{x(0,0)}(\pi,\pi^*)$ and $^1Q_{x(1,0)}(\pi,\pi^*)$ states. The FFT amplitude of 1040 cm^{-1}, which is the energy difference between $Q_x(1,0)$ and $Q_x(0,0)$ band, was proportional to the pump intensity as shown in Figure 9. The ratio of the excited population density between $Q_x(0,0)$ and $Q_x(1,0)$ was calculated to be 1.92:1 from the absorption and laser spectra. The signals due to $^1Q_{x(1,0)}(\pi,\pi^*)$ and $^1Q_{x(0,0)}(\pi,\pi^*)$ are thought to decay in a sequential order from the higher energy states to the lower energy states in the sequences $^1Q_{x(1,0)}(\pi,\pi^*) \rightarrow {}^1Q_{x(0,0)}(\pi,\pi^*) \rightarrow {}^3(d,\pi^*) \rightarrow {}^3(\pi,\pi^*)$ and $^1Q_{x(0,0)}(\pi,\pi^*) \rightarrow {}^3(d,\pi^*) \rightarrow {}^3(\pi,\pi^*)$. The real-time ΔA traces are expected to be fitted well with the following equation.

$$\begin{aligned} f(t) &= (1.92/2.92)[(A_1(\exp(-t/\tau_1)) + A_2(\exp(-t/\tau_2) - \exp(-t/\tau_1)) + A_3(\exp(-t/\tau_3) - \exp(-t/\tau_2)) + A_4(1 - \exp(-t/\tau_3))] + (1/2.92)[A_2(\exp(-t/\tau_2) - \exp(-t/\tau_1)) + A_3(\exp(-t/\tau_3) - \exp(-t/\tau_2)) + A_4(1 - \exp(-t/\tau_3))] \\ &= (1.92/2.92)(A_1(\exp(-t/\tau_1)) + A_2(\exp(-t/\tau_2) - \exp(-t/\tau_1)) + A_3(\exp(-t/\tau_3) - \exp(-t/\tau_2)) + A_4(1 - \exp(-t/\tau_3)) \end{aligned} \quad (1)$$

The spectra of components A_1, A_2, A_3, and A_4 thus obtained are shown in Figure 10. The signal of A_2, which has a negative peak at $\lambda_{max} = 591$ nm, is attributed to the stimulated emission from $^1Q_{x(0,0)}(\pi,\pi^*)$, based on its agreement with the stimulated emission spectrum ($\lambda_{max} = 595$ nm, Figure 10) calculated from the fluorescence spectrum (Supporting Information, Figure S1). Therefore, the lifetime of $^1Q_{x(0,0)}(\pi,\pi^*)$ was estimated to be 1150 fs ($=\tau_2$).

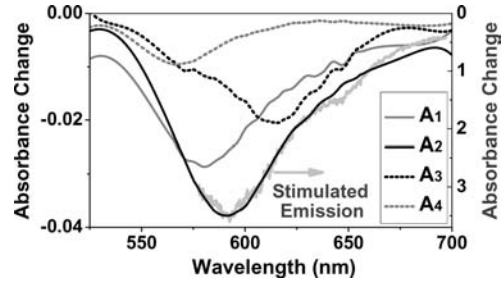

Figure 10. Spectra of four components obtained by the sequential model.

Spectrum A_1 has a negative peak at $\lambda_{max} = 580$ nm, which is 11 nm shorter than that of A_2. Both the negative peaks are reasonably attributed to stimulated emission because of impossible assignment to the bleaching due to the lack of absorption in the spectral range and from the peak wavelength close to that of the spontaneous emission spectrum. Therefore, A_1 can be attributed to the stimulated emission from $^1Q_{x(1,0)}(\pi,\pi^*)$ with a lifetime of 230 fs ($=\tau 1$). The lifetime of the A_1 signal is shorter than that of A_2. The reason why the peak wavelength of the stimulated emission band A_1 is shorter than that of A_2 can be explained as follows. The minimum of potential energy surface of excited state is displaced from that of the ground state. Therefore, $Q_x(1,0)$ can have not only the transition of $\nu_1' \rightarrow \nu_1$, but also higher energy transitions ($\nu_1' \rightarrow \nu_0$) and lower energy transitions ($\nu_1' \rightarrow \nu_2$ and $\nu_1' \rightarrow \nu_3$). In the same way, in the case of $Q_x(0,0)$, the transfer can not only be $\nu_0' \rightarrow \nu_0$ but also lower energy transitions like $\nu_0' \rightarrow \nu_1$ and $\nu_0' \rightarrow \nu_2$. The transfer energies of $\nu_0' \rightarrow \nu_0$ and $\nu_1' \rightarrow \nu_1$ are close to each other because both of $Q_x(1,0)$ and $Q_x(0,0)$ belong to the same electronic state in the lowest vibrational levels expected to have minimal anharmonicity. Among all of the possible transitions, $\nu_1' \rightarrow \nu_0$ is the only one transition which has higher transition energy than $\nu_0' \rightarrow \nu_0$ and $\nu_1' \rightarrow \nu_1$; therefore it is thought to be contributing the blue shift of A_1, which has a peak at 11 nm shorter than that of A_2. As mentioned above the lifetime of A_1 due to $^1Q_{x(1,0)}(\pi,\pi^*)$ is determined to be 230 $\pm$ 70 fs. This result is in relatively good agreement with the step-down time of 190 $\pm$ 40 fs for the transition time from $^1Q_{x(1,0)}(\pi,\pi^*)$ to $^1Q_{x(0,0)}(\pi,\pi^*)$ calculated from the energy decay rate in the dynamic Stokes-shift process. Moreover, the hypothesis of the spectral component A_1 being due to the stimulated emission from $^1Q_{x(1,0)}(\pi,\pi^*)$ is supported by the following observed phenomena. The ratio between FWHMs of A_1 [related to $Q_x(1,0)$] and A_2 [related to $Q_x(0,0)$] was determined to be 58.6nm/49.6 nm = 1.2 $\pm$ 0.1 (Figure 10). While, the ratio between FWHMs of $Q_x(1,0)$ and $Q_x(0,0)$ bands in the UV/vis spectra was 33.5 nm/23.2 nm = 1.44 $\pm$ 0.02 (Figure 8). The observation that A_2 has a broader bandwidth than A_1 is consistent with the $Q_x(1,0)$ band being broader than the $Q_x(0,0)$ band.

The component A_3, which has a negative peak at $\lambda_{max} =$ 616 nm and the longer lifetime than A_2, is concluded to be due to the stimulated emission from the triplet excited state as follows. The intersystem crossing from $^1(\pi,\pi^*)$ to $^3(d,\pi^*)$ is thought to take place more easily than the spin-forbidden intersystem crossing from $^1(\pi,\pi^*)$ to $^3(\pi,\pi^*)$.[9] Moreover, the

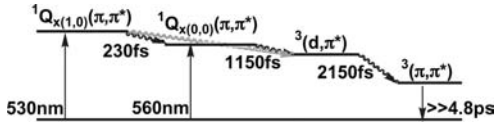

Figure 11. Energy level diagram illustrating the excited-state dynamics.

charge transfer from the porphyrin ring to the central metal atom enhances the spin−orbit coupling and accelerates intersystem crossing. Therefore, the A_3 spectrum with a peak at $\lambda_{max} = 616$ nm is due to a stimulated emission signal from $^3(d,\pi^*)$. This assignment is also supported by previous reports showing that the phosphorescence from $^3(\pi,\pi^*)$ has a $\lambda_{max} = 725$ nm in Ru(tpp)(CO)Py[3] and $^3(d,\pi^*)$ exists close to $^1(\pi,\pi^*)$ between $^1(\pi,\pi^*)$ and $^3(\pi,\pi^*)$.[2b] It is at first sight surprising that the stimulated emission from the triplet state appears with intensity of about 1/2 of that of the stimulated emission from the singlet state. However, the signal cannot be assigned to the stimulated emission from the singlet state because the signal appears in the region whose wavelength is longer than that of the spontaneous emission from the singlet state. Therefore, the signal can only be assigned to the stimulated emission from the triplet state. There is no report concerning the S-T absorption of Ru porphyrin complex, whose lowest triplet excited state is (π,π^*), but strong S-T absorption is reported in similar complexes such as Os porphyrin complex and the Ru bipyridine complex which have (d,π^*) as their lowest triplet excited states.[2c,12] It suggests the possibility of stimulated emission from $^3(d,\pi^*)$ of Ru^{II}(TPP)(CO). Moreover, besides strong stimulated emission, there exists the induced absorption from the excited singlet state and the excited triplet state. This can be the reason why the intensity of A_2 is 2 times or more larger than that of A_3. Therefore, the lifetime of $^3(d,\pi^*)$ was estimated to be about 2.2 ps ($=\tau_3$).

The component A_4, with a negative peak at $\lambda_{max} = 565$ nm, is due to residual (22%) bleaching induced by ground-state depletion remaining even at the longest delay, because Ru^{II}(TPP)(CO) has a $Q_x(0,0)$ absorption band in this spectral range around 565 nm ($\Delta A = 0.04$). The phosphorescence from $^3(\pi,\pi^*)$ is reported to have a peak at $\lambda_{max} = 725$ nm in Ru(tpp)(CO)Py,[3a] therefore the signal observed around 565 nm after relaxation to $^3(\pi,\pi^*)$ is not due to stimulated emission corresponding to the phosphorescence.

The results of the above analysis and discussion of the electronic state are summarized as follows; the lifetimes of $^1Q_{x(1,0)}(\pi,\pi^*)$, $^1Q_{x(0,0)}(\pi,\pi^*)$, $^3(d,\pi^*)$, and $^3(\pi,\pi^*)$ were determined to be 230 ± 70 fs, 1150 ± 260 fs, 2150 ± 360 fs, and ≫4.8 ps, respectively (Figure 11).

As a further proof of the mechanism of the decay dynamics of the intermediate states obtained above, the dynamics of the vibrational state were also analyzed. Using spectrogram analysis, we detected the transitional changes of these molecular vibration modes up to 1500 fs (Figure 12). The spectrogram was calculated from the averaged ΔA traces over 10 probe wavelengths around 600 nm using the Blackman window function whose fwhm was 240 fs. The data in the vicinity of 0 fs up to 300 fs could not be measured accurately because of the strong interference between the scattered pump pulse and probe pulse, and hence the results of the spectrogram analysis were shown in the delay time range from 300 to 1500 fs, where the effect of interference is negligibly small. At 300 fs, the porphyrin ring stretching mode (ν_{por}) was observed around 1036 cm^{-1}, which agrees well with the calculated frequency (1040 cm^{-1}) of singlet state Ru^{II}(por)(CO) [Figure 13a].[13] (The calculation method and its detailed results are shown in the Supporting Information.) This frequency is increased to 1150 cm^{-1} in several hundred fs from about 600 fs to 1 ps, because of the appearance of the triplet state, whose ν_{por} was obtained by the quantum chemical calculation to be 1100 cm^{-1}. The peak centered around 900 cm^{-1} that appears at ∼1 ps is also considered to be due to the triplet state after the intersystem crossing, because the calculated result suggests the appearance of the porphyrin ring bending mode at 990 cm^{-1}, characteristic of the triplet state in Ru^{II}(por)(CO) [Figure 13b]. From the relation in dynamics between the spectrogram and the electronic state analysis, we could thus clarify the ultrafast dynamics of Ru^{II}(TPP)(CO), which shows that the lifetime of the singlet excited state is about 1.2 ± 0.2 ps. Both positive and negative absorbance changes were successfully assigned to the absorption bands of the transition states.

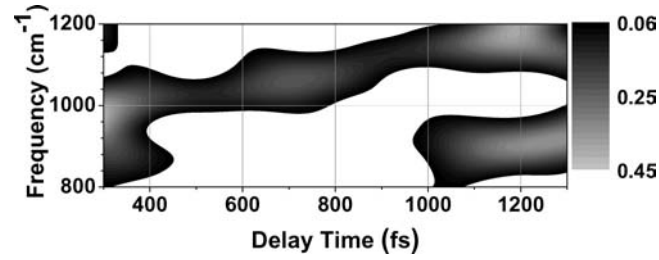

Figure 12. Fourier power spectrogram calculated from the real-time trace probed around 600 nm. The frequency resolution of the spectrogram was estimated to be 30 cm^{-1}.

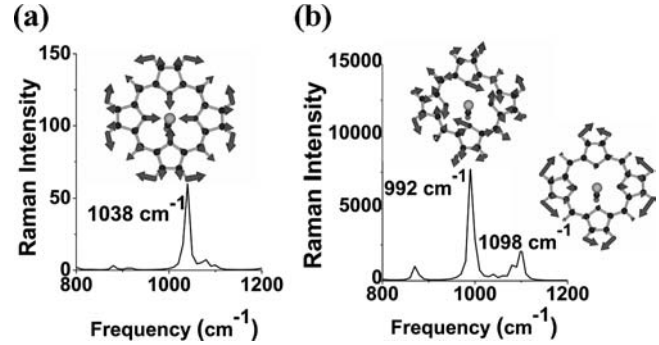

Figure 13. Calculated Raman spectra for (a) the ground singlet state and (b) the triplet state.

(12) (a) Funatsu, K.; Kimura, A.; Imamura, T.; Ichimura, A.; Sasaki, Y. *Inorg. Chem.* **1997**, *36*, 1625–1635. (b) Bhasikuttan, A. C.; Suzuki, M.; Nakashima, S.; Okada, T. *J. Am. Chem. Soc.* **2002**, *124*, 8398–8405.

(13) Geometry optimizations were performed with B3LYP/6-31G* for model RuII(CO)(por) (a) Frisch, M. J. *Gaussian 03, revision, D.02*; Gaussian, Inc.: Wallingford, CT, 2004. Details are shown in the Supporting Information. (b) Becke, A. D. *J. Chem. Phys.* **1993**, *98*, 5648–5652. (c) Lee, C.; Yang, W.; Parr, R. G. *Phys. Rev. B* **1988**, *37*, 785–789.

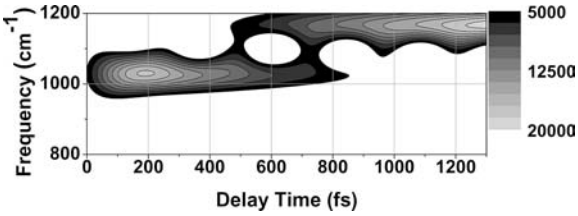

Figure 14. Simulated data of spectrogram assuming that the modes of 1040 and 1150 cm^{-1} decay and rise, respectively, with the same time constant of 1060 fs.

The electron spin state is thought to change from the singlet into the triplet state with a certain transition probability; therefore, we performed a model calculation in which the Fourier power of the porphyrin ring stretching mode of 1040 cm^{-1} (singlet) and that of 1150 cm^{1} (triplet) decays and grows, respectively, both with a time constant of 1.2 ps. The calculation shows the two frequency modes keeping their original frequencies (Figure 14). However, experimental results show the presence of intermixing as a gradual blue shift of ν_{por} from 1040 to 1150 cm^{-1}. The signal intensity at 1060 cm^{-1} has a peak at the gate delay time of 640 fs during the course of the delay time. This may be due to the bottleneck of wavepacket passage through the curve crossing point between the excited singlet state and the excited triplet state. The structural change in Ru^{II}(TPP)(CO) during the transition from the Franck−Condon state to the curve crossing point between the singlet and the triplet followed by the intersystem crossing to the triplet state.[14] The intersystem crossing takes place with a time constant of about 1 ps. This ultrafast intersystem crossing is due to the heavy atom effect of Ru on the spin−orbit coupling and/or the mediation of high-frequency modes of the molecule in a strong non-Born−Oppenheimer regime as reported by Chergui et al.[15]

In conclusion, both electronic relaxation and vibrational dynamics in Ru^{II}(TPP)(CO) were elucidated simultaneously under the same experimental conditions using a sub-5 fs pulse. From the observed electronic dynamics of Ru^{II}(TPP)(CO), the lifetimes of $^1Q_{x(1,0)}(\pi,\pi^*)$ and $^1Q_{x(0,0)}(\pi,\pi^*)$ were determined to be 230 ± 70 fs and 1150 ± 260 fs, respectively. Moreover, observed dynamic changes in the vibrational spectrum of ν_{por} from 1040 to 1150 cm^{-1} were identified to be a change in the spin state from the excited singlet state to the triplet state during the transition from the Franck−Condon state to the curve crossing point between the singlet and the triplet. The time constant of the intersystem crossing was successfully determined to be 1.2 ± 0.2 ps, and detailed vibration dynamics were clarified in the intersystem crossing dynamics.

Acknowledgment. This work was supported by Grant-in-Aid for JSPS Fellows to I.I., the grant from the Ministers of Education in Taiwan under the ATU Program at the National Chiao-Tung University to A.Y. and T.K, and the 21st Century COE program on "Coherent Optical Science" to T.K. The authors are grateful to the Information Technology Center of the University of Electro-Communications and the Information Technology Center of the University of Tokyo for their support of the DFT calculations.

Supporting Information Available: Fluorescence spectrum of Ru^{II}(TPP)(CO) and calculation results. This material is available free of charge via the Internet at http://pubs.acs.org.

IC801477A

(14) The metal-complex structure change during the chemical reaction causes the intersystem crossing (a) Danovich, D.; Shaik, S. J. *J. Am. Chem. Soc.* **1997**, *119*, 1773–1786. (b) Khavrutskii, I. V.; Musaev, D. G.; Morokuma, K. *Inorg. Chem.* **2003**, *42*, 2606–2621. (c) Iwakura, I.; Ikeno, T.; Yamada, T. *Angew. Chem., Int. Ed.* **2005**, *44*, 2524–2527. (d) Wang, Y.; Yang, C.; Wang, H.; Han, K.; Shaik, S. *Chem. Bio. Chem.* **2007**, *8*, 277–281.

(15) The heavy-atom effect is reported not to be a critical parameter in intersystem crossing of ^{1}MLCT→^{3}MLCT of M(bpy)$_3$ complex in ref (a−d). On the other hand, the heavy-atom effect was observed in intersystem crossing of $1(\pi,\pi^*)\rightarrow^3(\pi,\pi^*)$ of M protoporphyrin in ref (e). The existence of the heavy atomic effect is not sure in the present work of $1(\pi,\pi^*)\rightarrow^3(d,\pi^*)$. Therefore, just a possibility of the heavy atomic effect was mentioned in the manuscript (a) Cannizzo, A.; Mourik, F.; Gawelda, W.; Zgrablic, G.; Bressler, C.; Chergui, M. *Angew. Chem., Int. Ed.* **2006**, *45*, 3174–3176. (b) Gawelda, W.; Cannizzo, A.; Pham, V.-T.; Mourik, F.; Bressler, C.; Chergui, M. *J. Am. Chem. Soc.* **2007**, *129*, 8199–8206. (c) Cannizzo, A.; Blanco-Rodriguez, A. M.; Nahhas, A. E.; Sebera, J.; Zalis, S.; Vlcek, A. Jr.; Chergui, M. *J. Am. Chem. Soc.* **2008**, *130*, 8968–8974. (d) Bressler, Ch.; Milne, C.; Pham, V.-T.; ElNahhas, A.; van der Veen, R. M.; Gawelda, W.; Johnson, S.; Beaud, P.; Grolimund, D.; Kaiser, M.; Borca, C. N.; Ingold, G.; Abela, R.; Chergui, M. *Science* **2009**, *323*, 489–492. (e) Kobayashi, T.; Straub, K. D.; Rentzepis, P. M. *Photochem. Photobiol.* **1979**, *29*, 925–931.